Ann. Geophys., 28, 951–967, 2010
www.ann-geophys.net/28/951/2010/

Annales Geophysicae

Low-frequency magnetic field fluctuations in Venus' solar wind interaction region: Venus Express observations

L. Guicking[1], K.-H. Glassmeier[1,2], H.-U. Auster[1], M. Delva[3], U. Motschmann[4,5], Y. Narita[1], and T. L. Zhang[3]

[1]Institut für Geophysik und extraterrestrische Physik, Technische Universität Braunschweig, Mendelssohnstrasse 3, 38106 Braunschweig, Germany
[2]Max-Planck-Institut für Sonnensystemforschung, Max-Planck-Strasse 2, 37191 Katlenburg-Lindau, Germany
[3]Space Research Institute, Austrian Academy of Sciences, Schmiedlstrasse 6, 8042 Graz, Austria
[4]Institut für Theoretische Physik, Technische Universität Braunschweig, Mendelssohnstrasse 3, 38106 Braunschweig, Germany
[5]Institut für Planetenforschung, Deutsches Zentrum für Luft- und Raumfahrt (DLR), Rutherfordstrasse 2, 12489 Berlin, Germany

Received: 2 October 2009 – Revised: 5 February 2010 – Accepted: 31 March 2010 – Published: 15 April 2010

Abstract. We investigate wave properties of low-frequency magnetic field fluctuations in Venus' solar wind interaction region based on the measurements made on board the Venus Express spacecraft. The orbit geometry is very suitable to investigate the fluctuations in Venus' low-altitude magnetosheath and mid-magnetotail and provides an opportunity for a comparative study of low-frequency waves at Venus and Mars. The spatial distributions of the wave properties, in particular in the dayside and nightside magnetosheath as well as in the tail and mantle region, are similar to observations at Mars. As both planets do not have a global magnetic field, the interaction process of the solar wind with both planets is similar and leads to similar instabilities and wave structures. We focus on the spatial distribution of the wave intensity of the fluctuating magnetic field and detect an enhancement of the intensity in the dayside magnetosheath and a strong decrease towards the terminator. For a detailed investigation of the intensity distribution we adopt an analytical streamline model to describe the plasma flow around Venus. This allows displaying the evolution of the intensity along different streamlines. It is assumed that the waves are generated in the vicinity of the bow shock and are convected downstream with the turbulent magnetosheath flow. However, neither the different Mach numbers upstream and downstream of the bow shock, nor the variation of the cross sectional area and the flow velocity along the streamlines play probably an important role in order to explain the observed concentration of wave intensity in the dayside magnetosheath and the decay towards the nightside magnetosheath. But, the concept of freely evolving or decaying turbulence is in good qualitative agreement with the observations, as we observe a power law decay of the intensity along the streamlines. The observations support the assumption of wave convection through the magnetosheath, but reveal at the same time that wave sources may not only exist at the bow shock, but also in the magnetosheath.

Keywords. Magnetospheric physics (MHD waves and instabilities; Solar wind interactions with unmagnetized bodies) – Space plasma physics (Turbulence)

1 Introduction

Waves in plasmas, which are generally considered as fluctuations in the electric field, the magnetic field, the density, and the temperature, play an important role in the interaction processes of the solar wind with planets and other solar system bodies. Because the particle densities in space plasmas surrounding the obstacles are low, collisions between particles occur rarely and the transfer of momentum and energy can only be accomplished by waves. Hence, it is important to study wave characteristics, their origins, and generation mechanisms in order to improve our understanding of the complex interaction processes. Many observations of waves in the ultra-low-frequency and low-frequency range at various planets are reported (e.g. Glassmeier and Espley, 2006). Above all, it is interesting to study the plasma environment

Correspondence to: L. Guicking
(l.guicking@tu-bs.de)

of Venus, because it does not possess an intrinsic magnetic field and the solar wind interaction is similar to that at Mars (e.g. Cloutier et al., 1999), also lacking a global planetary magnetic field (e.g. Acuña et al., 1998). A statistical study of low-frequency magnetic field oscillations in the Martian plasma environment is presented by Espley et al. (2004).

Since the early 1960s Venus has been an object of exploration by more than 20 spacecraft missions from the United States and the former Soviet Union. However, most of the current understanding of the solar wind interaction with Venus comes from the Pioneer Venus Orbiter (PVO) due to its long-lasting mission from 1978 to 1992 (Russell, 1991). At Venus the solar wind interacts directly with the planet's upper atmosphere, creating various boundaries and regions in the Venusian plasma environment (e.g. Luhmann, 1986). Observations of plasma waves, mainly detected by the Orbiter Electric Field Detector (OEFD) on board the PVO at frequencies from 100 Hz to 30 kHz are summarised by Huba and Strangeway (1997) and Strangeway (1991) and are compared to observations at Mars by Strangeway (2004). The temporal resolution of the PVO magnetometer samples reaches 12 Hz (Russell et al., 1980) and thus allows to investigate magnetic field fluctuations up to a few Hz. Waves upstream of the Venusian bow shock have been studied by Orlowski et al. (1994) and Strangeway and Crawford (1995). Downstream of the bow shock Brace et al. (1983) detected ionospheric wave structures nightward of the terminator which they call post-terminator ionospheric waves. Large magnetic field fluctuations in the magnetosheath of Venus with periods from 10 to 40 s have been observed by Luhmann et al. (1983). They supposed that these waves are generated most likely in the vicinity of the quasi-parallel bow shock and are convected downstream in the magnetosheath with the solar wind plasma. Their possible origin has been studied by means of numerical simulations by Winske (1986), suggesting that plasma instabilities can generate these waves either directly by the interaction of the solar wind with the quasi-parallel bow shock or with the oxygen ions of planetary origin (pickup ions). Luhmann (1995) investigated magnetic field fluctuations in the low-altitude subsolar magnetosheath and found predominantly linearly polarised waves of transverse character with regard to the background magnetic field which have also been observed at Earth. Grebowsky et al. (2004) observed ultra-low-frequency waves in the vicinity of detected ion pickup regions which suggest an association of wave generation with the pickup ions.

The current knowledge about Venus and its space environment is now further completed by the Venus Express spacecraft, the first European mission to the planet Venus (Titov et al., 2006). Launched in November 2005, the spacecraft arrived at Venus in April 2006 and was inserted into a polar orbit with a period of 24 h. The orbit geometry of Venus Express allows magnetic field measurements in the low-altitude region near the terminator and the mid-magnetotail region which were not covered by the PVO (Zhang et al., 2006). The better coverage of the Venusian dayside and nightside magnetosheath as well as the magnetotail provides an opportunity to study statistically magnetic field fluctuations in these regions in more detail. Recently, proton cyclotron waves upstream of the Venusian bow shock (Delva et al., 2008a,b,c) and mirror mode structures in the magnetosheath (Volwerk et al., 2008a,b) have been detected using the magnetic field measurements of the fluxgate magnetometer on board the Venus Express spacecraft (Zhang et al., 2006). Vörös et al. (2008a,b) studied properties of magnetic field fluctuations in the Venusian magnetosheath and wake and observed varying scaling features of the fluctuations in the different regions.

In this work we present a statistical study of magnetic field fluctuations near Venus in the low-frequency regime. We adopt the definition given by Espley et al. (2004) who refer frequencies near or below the proton gyrofrequency as the low-frequency range and frequencies below the lowest local ion gyrofrequency as the ultra-low-frequency range. As Espley et al. (2004) provide a statistical study of low-frequency magnetic field oscillations at Mars, including the magnetosheath, the magnetic pileup region, and the tail, our study provides also the basis for a comparative wave study between Venus and Mars.

2 Data and analysis methods

In this study we use a Venus Express magnetometer data set which includes 567 orbits between April 2006 and December 2007 with a temporal resolution of 1 s. The data are corrected for perturbations caused by the spacecraft so that the data have an accuracy of about 1 nT for the absolute field and an accuracy better than 0.1 nT for the variable field. This accuracy has been realised by a novel software procedure applied to the dual-sensor measurements of the Venus Express magnetometer (Zhang et al., 2008a,c). The data set is given in the Venus solar orbital (VSO) coordinate system in which the x-axis points towards the sun, the y-axis is in the opposite direction to the planetary orbital motion and the z-axis completes the right-handed coordinate system pointing northward from the orbital plane. In order to take into account the orbital velocity of Venus with respect to the mean solar wind velocity, we adopt the aberrated VSO coordinate system (x',y',z') suggested by Martinecz et al. (2008) for the presentation of the results. The transformation to the aberrated VSO coordinate system (VSO' coordinate system) is realised by a constant rotation of 5° around the z-axis.

Figure 1 shows the spatial distribution of the observed magnetic field strength in a cylindrical coordinate system in which the magnetic field strength is averaged over the directions around the x'-axis. So, the cylindrical symmetry is assumed with regard to the x'-axis, leading to a two-dimensional picture with the axes $x'_{cyl} = x'$ and $y'_{cyl} = \sqrt{y'^2 + z'^2}$. This means that the x'_{cyl}-axis represents the apparent solar wind direction and the y'_{cyl}-axis the distance

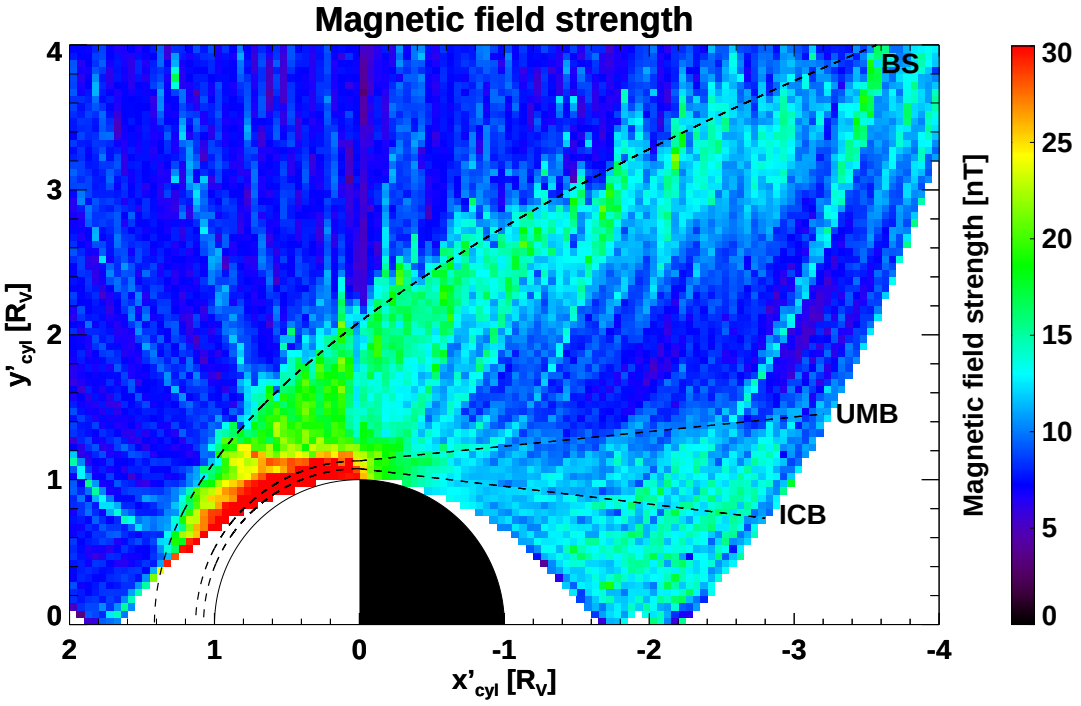

Fig. 1. Spatial distribution of the magnetic field strength in the plasma environment surrounding Venus. The measurements are averaged around the axis of the apparent solar wind direction (x'_{cyl}). Downstream of the bow shock (BS) the magnetic field strength is enhanced relative to the solar wind region upstream of the bow shock and piles up towards the terminator in the low-altitude dayside magnetosheath forming the magnetic barrier. Draping of the magnetic field around the planet leads to the formation of the magnetotail which is characterised by a slightly enhanced magnetic field strength in the planet's wake, too.

from the x'_{cyl}-axis (Martinecz et al., 2008). It is convenient to locate regions and boundaries at Venus. In Fig. 1 the data are presented in the range $2\,R_V \leq x'_{cyl} \leq -4\,R_V$ and $y'_{cyl} \leq 4\,R_V$ and each colour-coded bin has a size of $0.05\,R_V \times 0.05\,R_V$ (R_V: Venus radius). The locations of the bow shock (BS), the upper mantle boundary (UMB), and the ion composition boundary (ICB) determined by the models of Martinecz et al. (2009) are plotted for orientation and distinction of the different solar wind interaction regions, too. The magnetic field strength becomes enhanced downstream of the bow shock. This region downstream of the bow shock, between the bow shock and the UMB, is the so-called magnetosheath and characterised by slowed down and heated plasma with respect to the solar wind plasma upstream of the bow shock. The field piles up on the dayside of the planet and forms the magnetic barrier (Zhang et al., 2008b). The UMB and the ICB confine the mantle region which is characterised by a mixture of solar wind ions and ions of planetary origin. Below the ICB the solar wind protons disappear. Finally, the draping of the magnetic field lines around the planet leads to the formation of the magnetotail in which the magnetic field strength is also slightly enhanced compared to the strength upstream of the bow shock.

For our statistical study intervals with the time length 100 s are selected with a shift of 1 s from one interval to another. Gaps in the data set greater than 1.5 s are excluded from the analysis. The interval length is chosen as a trade-off between the temporal and spatial resolution as well as the occurrence of data gaps. With respect to the bin size that means that almost every bin is well covered by observations which is shown in Fig. 2. The statistical analysis is performed in the frequency range 30 to 300 mHz, as we focus on low-frequency magnetic field fluctuations. The lower boundary of this frequency range acts as a band-pass filter such that oscillations with periods longer than 33 s do not contribute to the statistical results. The gyrofrequency is defined as $\omega = qB/m$ where B is the magnetic field strength and q and m are the electric charge and the mass of the ion species. The upper boundary of the analysed frequency range, 300 mHz, corresponds to the proton gyrofrequency at a field strength of about 20 nT, a typical magnetic field strength in the Venusian magnetosheath (Fig. 1); therefore the frequency range well covers the low-frequency range in Venus' solar wind interaction region. In spite of that, we realise that it is also attractive to expand or reduce the frequency band depending on the conditions in specific regions (e.g. with respect to the gyrofrequency) which would allow a comparison of

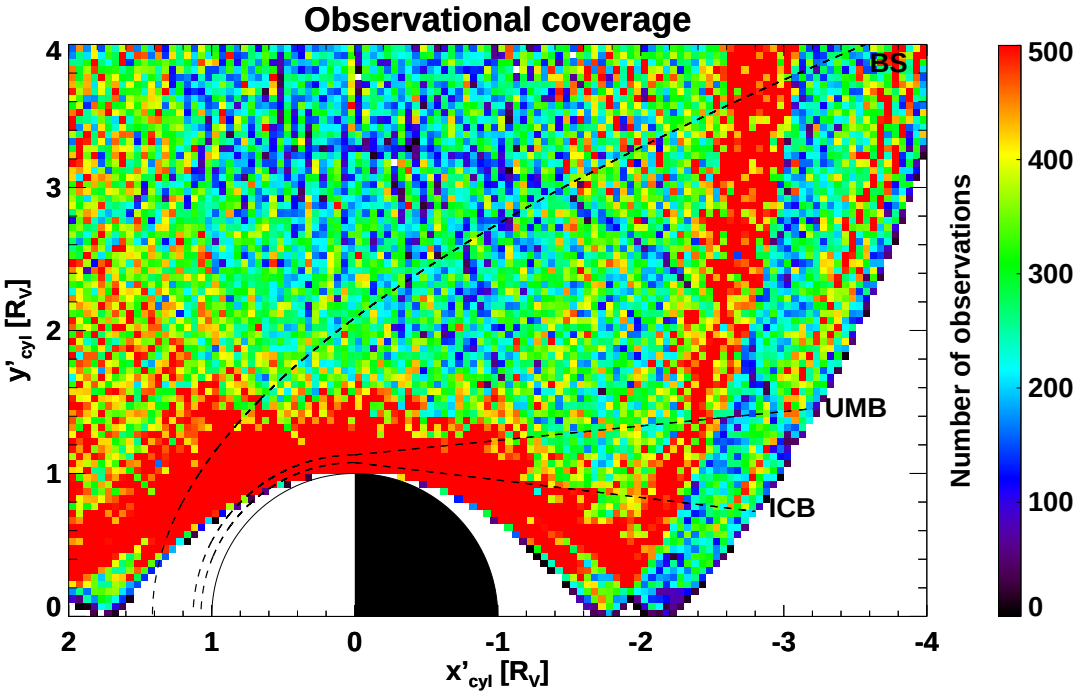

Fig. 2. Observational coverage. Almost every bin is well covered by observations, but the spatial distribution is not homogenous. The polar orbit of Venus Express provides in the vicinity of the pericentre relatively more observations.

different frequency bands. In particular, studying the ultra-low-frequency range in more detail would be worthwhile, but we mention again that increasing the frequency resolution is at the expense of the spatial resolution and is thus always a balancing issue.

Spectral analysis is widely used in order to determine wave properties such as the wave power, ellipticity, polarisation, and propagation direction. The wave analysis methods are well developed by e.g. Arthur et al. (1976); Samson (1973); McPherron et al. (1972); Means (1972); Sonnerup and Cahill (1967) and are frequently applied to space time series data. The methods are based on several assumptions and there are also limitations. First of all, the analysis method is based on the assumption of plane waves and there is an ambiguity of $\pm 180°$ in determining the propagation direction of the waves as one determines the minimum variance direction only. This comes from the fact that the magnetic field is measured by a single spacecraft. Furthermore, from single spacecraft measurements one can only determine wave parameters in the spacecraft frame of reference which is subject to the Doppler shift of frequencies, when the measurements are made in a flow. The analysis of a certain frequency band, finally, leads to averaged wave parameters for this frequency band.

The wave analysis is performed as follows: (1) The magnetic field components of each time interval are transformed to a mean field aligned (MFA) coordinate system in which the principal direction (z-axis) is defined as the direction of the mean magnetic field in the interval, the second direction (x-axis) is perpendicular to the plane spanned by the vector pointing into the new z-direction and the spacecraft position vector in VSO coordinates, and the third direction (y-axis) completes the right-handed coordinate system. This transformation allows us to distinguish between the transverse and the compressional power of the fluctuations with respect to the mean magnetic field. (2) The data in the MFA system are Fourier transformed into frequencies. (3) With the Fourier transform $\boldsymbol{B}(w)$ we calculate the power spectral density matrix $\mathbf{P}$ for the selected frequency range

$$P_{ij} = \langle B_i(w) B_j^*(w) \rangle, \tag{1}$$

where i and j are the three components of the magnetic field ($i, j = 1,2,3$) and the asterisk denotes the complex-conjugate. The power spectral density matrix is a 3×3 complex matrix and can therefore be written as the sum of its real and imaginary part ($P_{ij} = \mathrm{Re}(P_{ij}) + i\,\mathrm{Im}(P_{ij})$). In the MFA system two diagonal elements, P_{11} and P_{22}, represent an estimate of the transverse power, whereas P_{33} corresponds to the compressional power. (4) Finally, the principal axis analysis is applied in order to determine the minimum and maximum variance directions. In particular, diagonalisation of the real part of the power spectral matrix yields three eigenvectors ($\boldsymbol{\xi}_1$,$\boldsymbol{\xi}_2$,$\boldsymbol{\xi}_3$) and three eigenvalues (λ_1,λ_2,λ_3) for the maximum, intermediate, and minimum variance directions, respectively. The matrix of the three eigenvectors $\mathbf{T}$ can then

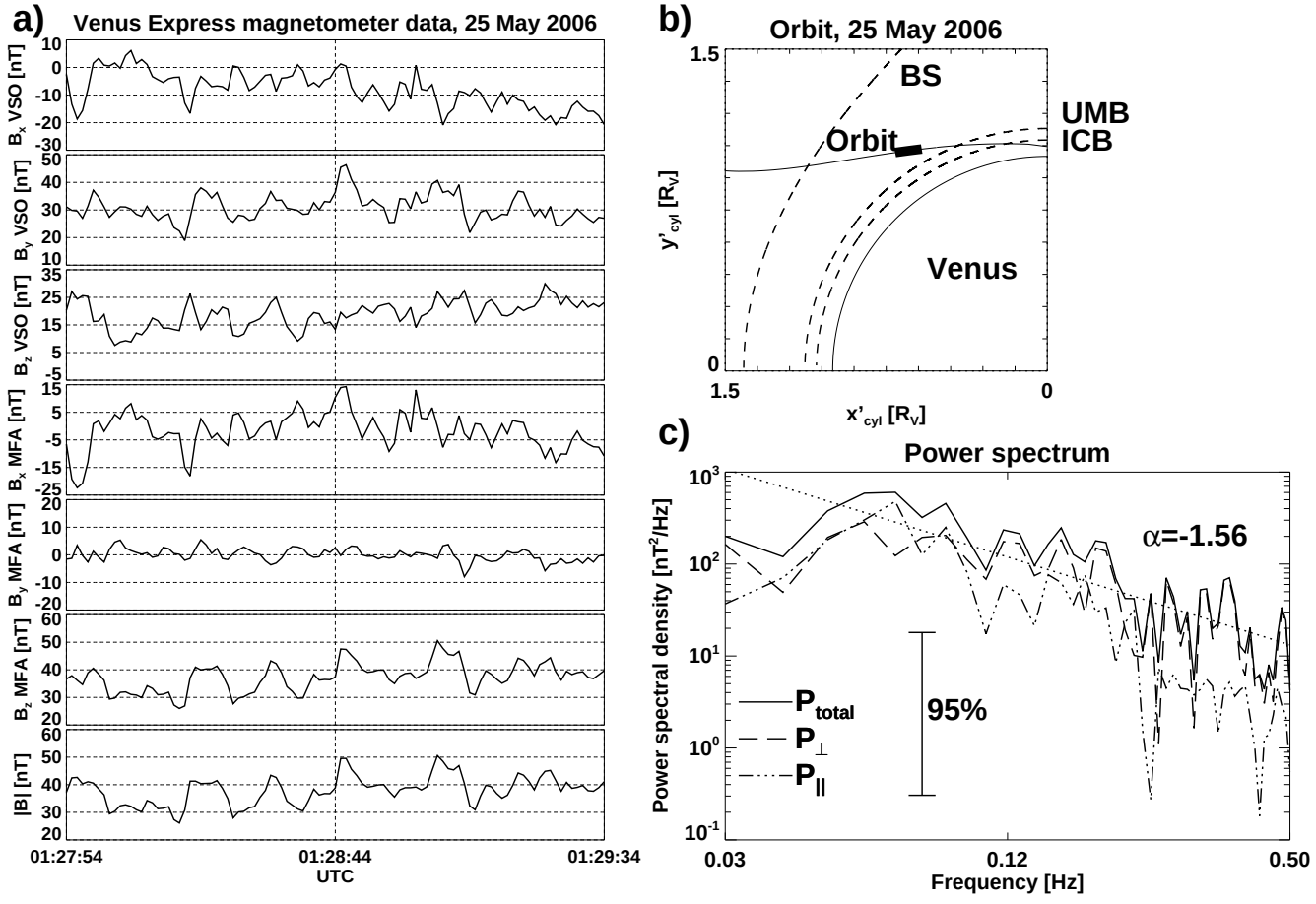

Fig. 3. Example of the analysis in the interval from 01:27:54 UTC to 01:29:34 UTC on 25 May 2006: **(a)** displays the three components of the magnetic field in VSO and MFA coordinates as well as the magnetic field strength. The mean magnetic field strength is 38 nT corresponding to the proton gyrofrequency $f_{\mathrm{gyro}} = 580$ mHz; **(b)** shows a sketch of the orbit in the dayside plasma environment close to Venus in cylindrical VSO′ coordinates. The black rectangle denotes the analysed time interval; **(c)** shows the power spectra of the magnetic field data in the frequency range from 30 to 500 mHz of the total power (P_{total}) as well as the transverse ($P_{\perp}$) and the compressional ($P_{\parallel}$) component (here a window function is applied to the spectra in order to increase the significance of the structures, but the spectra do not exhibit spectral peaks larger than the 95% confidence interval in this single spectrum). The dotted straight line indicates a linear fit in the logarithmic scaled spectrum revealing the spectral index $\alpha = -1.56$.

be used to transform the entire spectral matrix **P** into the principal axis (PA) system via $\mathbf{P}' = \mathbf{T}^{-1}\mathbf{P}\mathbf{T}$. Various wave properties are derived from the spectral matrix, the eigenvectors, and the eigenvalues and the results are presented in the following section. Here one should note that the propagation direction of the wave is well determined only if the intermediate eigenvalue is sufficiently larger than the minimum eigenvalue, otherwise the fluctuations are isotropic and the polarisation plane is not clearly determined.

3 Results

The analysis procedure in the previous section is demonstrated for one interval (25 May 2006, 01:27:54 UTC–01:29:34 UTC). In this time interval Venus Express is located in the high-latitude dayside magnetosheath. Figure 3 shows the magnetic field components in VSO (first to third panel in Fig. 3a) and MFA coordinates (fourth to sixth panel in Fig. 3a) as well as the magnetic field strength (bottom panel in Fig. 3a), the orbit trajectory in the cylindrical VSO′ coordinate system (Fig. 3b) and the power spectrum (Fig. 3c). The mean magnetic field is 38 nT corresponding to the proton gyrofrequency $f_{\mathrm{gyro}} = 580$ mHz.

The field components in the MFA coordinate system are Fourier transformed and the transverse Power $P_{\perp}$ and the compressional power $P_{\parallel}$ are determined from the power spectral density matrix.

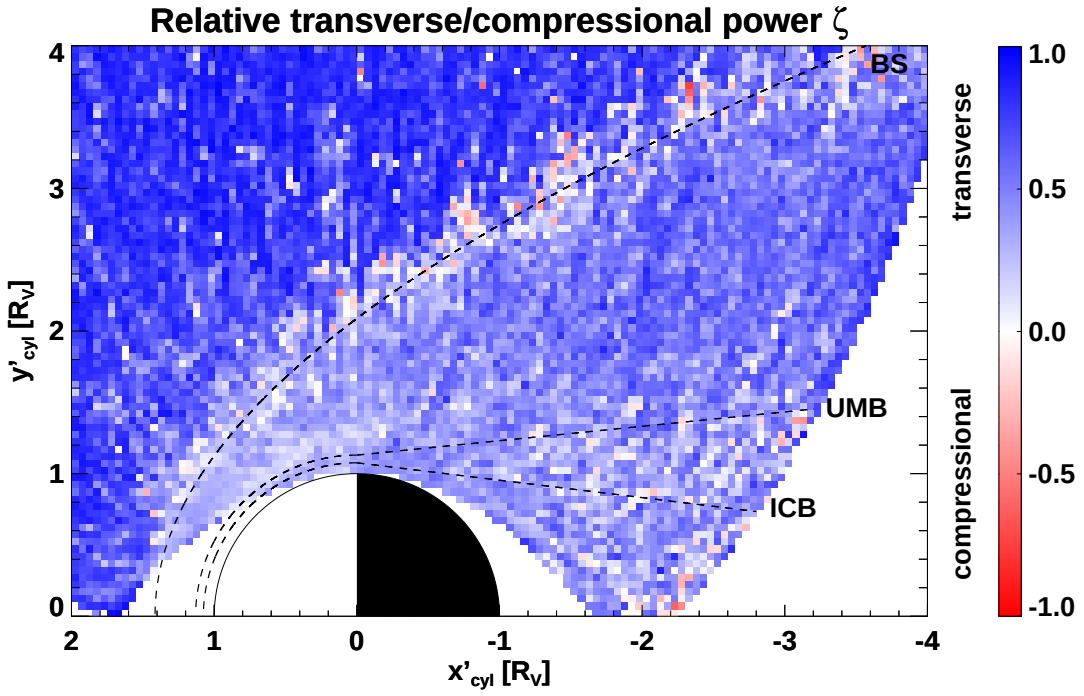

Fig. 4. Difference between the transverse and compressional power normalised to the total power about the mean field. The coordinate system is the same as in Fig. 1. Blue regions indicate regions where the transverse power dominates ($\zeta = +1$ purely transverse) and red regions where the compressional power dominates ($\zeta = -1$ purely compressional). In the vicinity of the dayside bow shock the magnitude of transverse and compressional power are of the same size, whereas in the vicinity of the nightside bow shock the compressional portion increases. In the dayside magnetosheath as well as in the mantle and tail region the compressional power is slightly higher than the compressional power in the nightside magnetosheath. In the solar wind upstream of the bow shock the transverse portion of the power dominates over the compressional portion.

We furthermore define the quantity ζ as

$$\zeta = \frac{P_\perp - P_\parallel}{P_{\text{total}}} \tag{2}$$

which is positive in the case of dominating transverse power and negative in the case of dominating compressional power. In the example interval we obtain the value $\zeta = 0.31$, therefore the transverse power exceeds the compressional one. This can also be seen in the power spectrum plot (Fig. 3c) in which the dashed line represents the transverse power spectral density $P_\perp$ and the dashed-dotted line the compressional power $P_\parallel$. After rotation into the PA coordinate system, we obtain further parameters describing the wave properties, namely the ellipticity, the sense of polarisation, the propagation directions, and the intensity. The absolute value of the ellipticity $|\epsilon|$ can be determined from the eigenvalues and is defined as (Song and Russell, 1999)

$$|\epsilon| = \sqrt{\frac{\lambda_2 - \lambda_3}{\lambda_1 - \lambda_3}} \tag{3}$$

assuming isotropic noise which means that λ_3 corresponds to the noise in the $\boldsymbol{k}$-direction. The sign of ϵ is the same as the sign of $\text{Im}(P'_{12})$. The average sense of polarisation over the frequency band yields the value $\epsilon = -0.72$ which indicates a slightly increased left-handed polarisation for the selected frequency band. Furthermore, the angle between the minimum variance direction and the mean magnetic field is about 90°, so the wave vector direction is practically perpendicular to the mean magnetic field. Finally, the intensity of the fluctuations I is defined as (Song and Russell, 1999)

$$I = \lambda_1 + \lambda_2 - 2\lambda_3. \tag{4}$$

The intensity is a mean spectral density of the chosen frequency band and we obtain $I = 157.2\,\text{nT}^2/\text{Hz}$. The intensity is an estimate of the total magnetic energy density in the frequency range 30 to 300 mHz. In summary, the analysis of the wave properties in this example exhibits dominating transverse, slightly left-handed polarised fluctuations with a large propagation angle relative to the mean field and enhanced wave intensity. We apply this analysis procedure to all available time intervals of the data set. The spatial distributions of various wave parameters are presented in the same fashion as in Fig. 1.

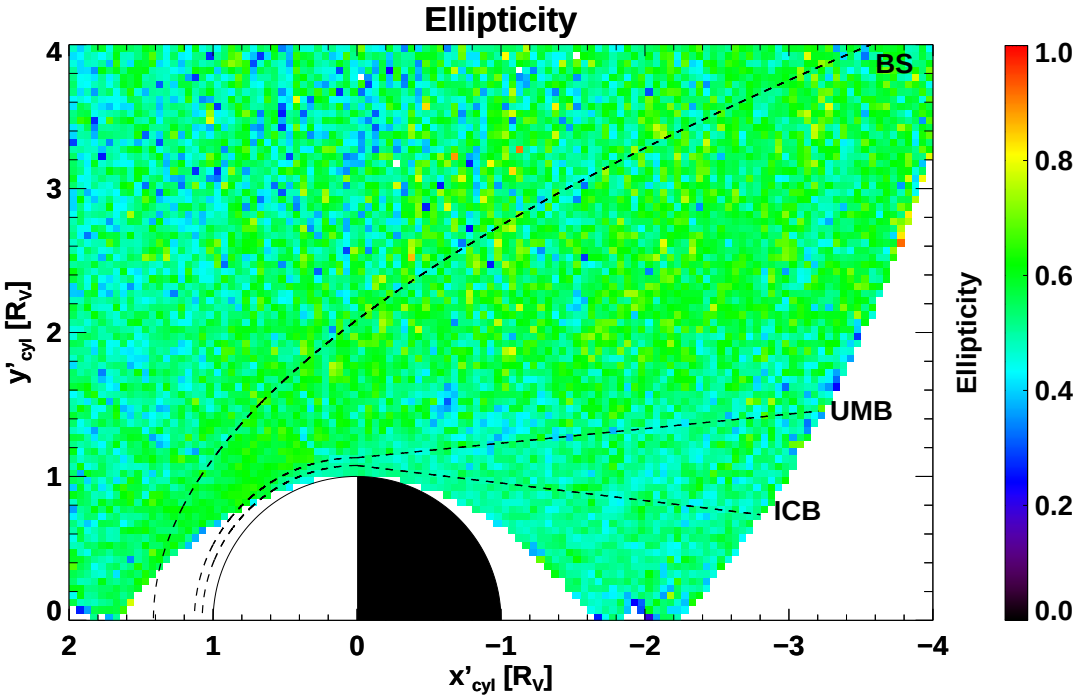

Fig. 5. Ellipticity of the waves in the space plasma environment surrounding Venus. The value $\epsilon = 0$ denotes a pure linear polarisation and $\epsilon = 1$ a pure circular polarisation.

3.1 Transverse vs. compressional power

Figure 4 displays the spatial distribution of the parameter ζ, the difference between the transverse and compressional power relative to the total power. Some features can be observed here: in the vicinity of the dayside bow shock the transverse and compressional power are almost equal, whereas the compressional power tends to be slightly greater in the vicinity of the nightside bow shock, because of the increased occurrence of red-coloured bins. However, by no means the compressional power clearly dominates this region. In the dayside magnetosheath as well as in the mantle and tail region the compressional power is slightly higher than that in the nightside magnetosheath. But the transverse power still exceeds the compressional power. In the solar wind (upstream of the bow shock) the transverse power dominates over the compressional one.

3.2 Ellipticity

The spatial distribution of the ellipticity is presented in Fig. 5. On average the absolute value of the ellipticity $|\epsilon|$ reaches higher values in the magnetosheath (around 0.6) with respect to the upstream solar wind and the tail and mantle region. Though, the waves are only moderately polarised, rarely exceeding the value 0.6, but also a few regions exist where the ellipticity is less than 0.6. In the upstream solar wind and in the mantle and tail region the ellipticity values are rather mixed and no clear tendency can be observed.

3.3 Polarisation

Figure 6 shows the spatial distribution of the average sense of polarisation of the low-frequency magnetic field fluctuations. The distribution does not show any clear distinct regions of either dominating left-handed or right-handed polarisation close to Venus. At larger distances from the planet there are areas of enhanced polarisation. However, neither the magnetosheath nor the tail and mantle region show large-scale connected areas with a preferred sense of polarisation. It should also be noted that for almost linear polarisation it is not meaningful to discuss the sense of polarisation due to the error in the determination of the ellipticity; the results should be treated with care. Furthermore, direct comparisons to polarisations derived from theoretical studies can lead to misinterpretations, as the Doppler shift from the plasma frame to the spacecraft frame of reference may reverse the senses of polarisation. Waves which propagate downstream from the bow shock do not change the polarisation. This is only the case if the waves propagate in opposite direction to the solar wind flow with a phase velocity lower than the solar wind flow velocity (e.g. Hoppe and Russell, 1983). In this context one should note that on the one hand averaging over the absolute values of the ellipticity may shift the average of a bin away from zero, but on the other hand a reversal

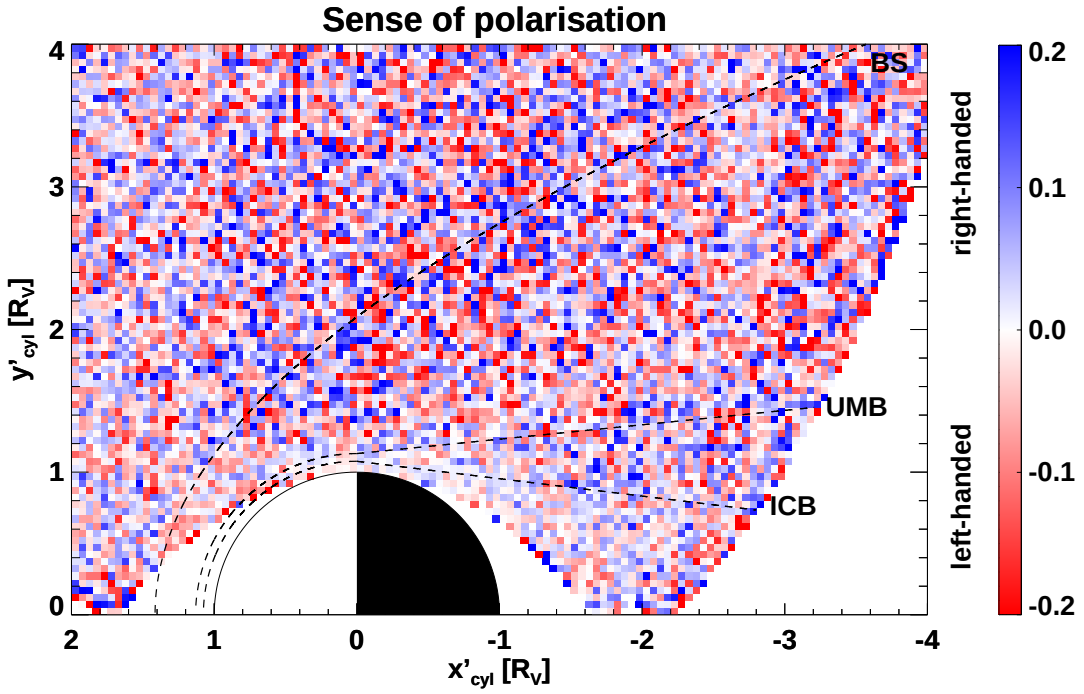

Fig. 6. Average sense of polarisation of the low-frequency magnetic field fluctuations in Venus' space plasma environment. Blue colours indicate regions of dominating right-handed polarisation and red colours regions of dominating left-handed polarisation. Close to the planet a tendency to less distinct regions of either preferentially left-handed or right-handed polarised waves is observable. The other regions are locally dominated by right-handed or left-handed polarisation, but no connected areas of larger size with a preferential sense of polarisation is visible.

of the polarisation between the plasma frame and the spacecraft frame of reference could also act conversely. Therefore, some caution has to be exercised discussing the observations displayed in Figs. 5 and 6. With a single spacecraft we are not able to correct for the Doppler shift.

3.4 Wave vector direction

As already mentioned in Sect. 2, the determination of the propagation direction or the wave vector direction is valid only, when the ratio of the intermediate to the minimum eigenvalue (λ_2/λ_3) is large enough. Espley et al. (2004) used a ratio of 2 as a criterion in order to determine the wave vector direction of low-frequency magnetic field oscillations in the Martian plasma environment. We note that according to Song and Russell (1999) high ratios are favoured, because the propagation direction is better determined for higher ratios of the eigenvalues. Therefore, we use a more stringent condition than Espley et al. (2004) and consider only cases with the intermediate to minimum eigenvalue ratio greater than 5. This is a compromise, because otherwise we lose a significant portion of the data set in the analysis. We accept possible limitations so far as we give a statistical result. Figure 7 shows the spatial distribution of the angle between the wave vector and the mean magnetic field in Venus' solar wind interaction region in the cases satisfying the specified eigenvalue ratio criterion. In Fig. 7 one can see that in the low-altitude dayside magnetosheath the wave vector directions are almost perpendicular to the mean magnetic field. Also in the mantle and tail region a majority of the angles reaches values greater than 45°, whereas in the nightside magnetosheath a tendency to smaller angles can be observed, in particular, events with an angle below 45° occur quite frequently. Data gaps in the magnetosheath are due to the selection criterion of the intermediate to minimum eigenvalue ratio. In the upstream solar wind the results are fairly mixed with a slight predominance of angles greater than 45°.

3.5 Intensity

The spatial distribution of the wave intensity I about the mean field in the plasma environment surrounding Venus is presented in Fig. 8. The intensity is largest in the entire dayside magnetosheath and decreases rapidly towards the terminator region. In the nightside magnetosheath the intensity is still moderately enhanced in the vicinity of the bow shock, but further downstream and in the mantle and tail region only very small wave intensities can be observed. We would like to note that the lower end of the colour bar displaying the intensity in Fig. 8 is two orders of magnitude

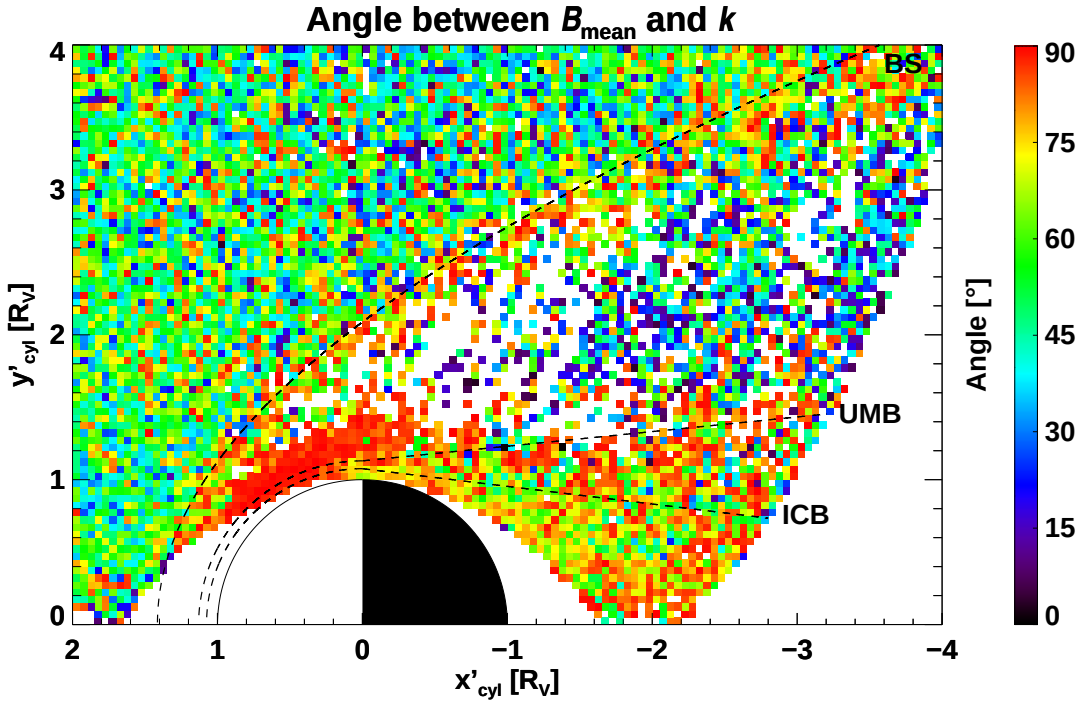

Fig. 7. Spatial distribution of the angles of the wave vector direction with respect to the mean magnetic field. Data gaps in the figure are due to the selection criterion of a ratio of the intermediate to the minimum eigenvalue greater than 5. The low-altitude dayside magnetosheath is characterised by the occurrence of large angles between the wave vector direction and the mean magnetic field. The tail and mantle region is dominated by angles greater than 45°, whereas in the nightside magnetosheath also smaller angles occur. In the upstream solar wind a wider distribution of angles is observed.

above the threshold of the data accuracy. Almost all intensities are above this threshold and therefore the artificial contribution to our results is expected to be very small. In regions with lower intensities the wave property results may be subject of a somewhat increased uncertainty compared to regions with larger intensities, though. The wave intensity distribution is further investigated and discussed in more detail in the next section, as it may give a hint about how rapidly turbulence evolves in the magnetosheath. This is of great interest in fundamental plasma physics.

3.6 Spectral indices

Power spectra for the both transverse and compressional fluctuations exhibit a power law spectrum in the analysed frequency range. From our statistical analysis we have determined the average spectral indices of the total, transverse, and compressional power in the magnetosheath, mantle, and tail region (Table 1) providing an estimate of the different turbulent states. The spectral indices of the total power in the dayside and nightside magnetosheath are slightly flatter than in the mantle and tail region. Furthermore, in the dayside and nightside magnetosheath as well as in the mantle the spectral indices of the compressional component are steeper than the transverse ones. In the tail the decay of the transverse component is steepest.

4 Discussion

The statistical analysis reveals the wave properties of the low-frequency magnetic field fluctuations in various Venusian solar wind interaction regions. The observations are summarised and compared to the wave properties observed at Mars. We also investigate the spatial distribution of the intensity in more detail and discuss possible mechanisms and processes which may lead to the made observations.

4.1 Wave properties at Venus and Mars

In the dayside magnetosheath and the vicinity of the bow shock the compressional and transverse power are approximately equal and the waves are moderately elliptically polarised with changing senses of polarisation. With larger distances from the planet the respective polarisation increases. Closer to the planet the senses of polarisation are not much pronounced. The wave vector has largest angles with respect to the mean magnetic field in the low-altitude magnetosheath and smaller angles at higher altitudes. The wave

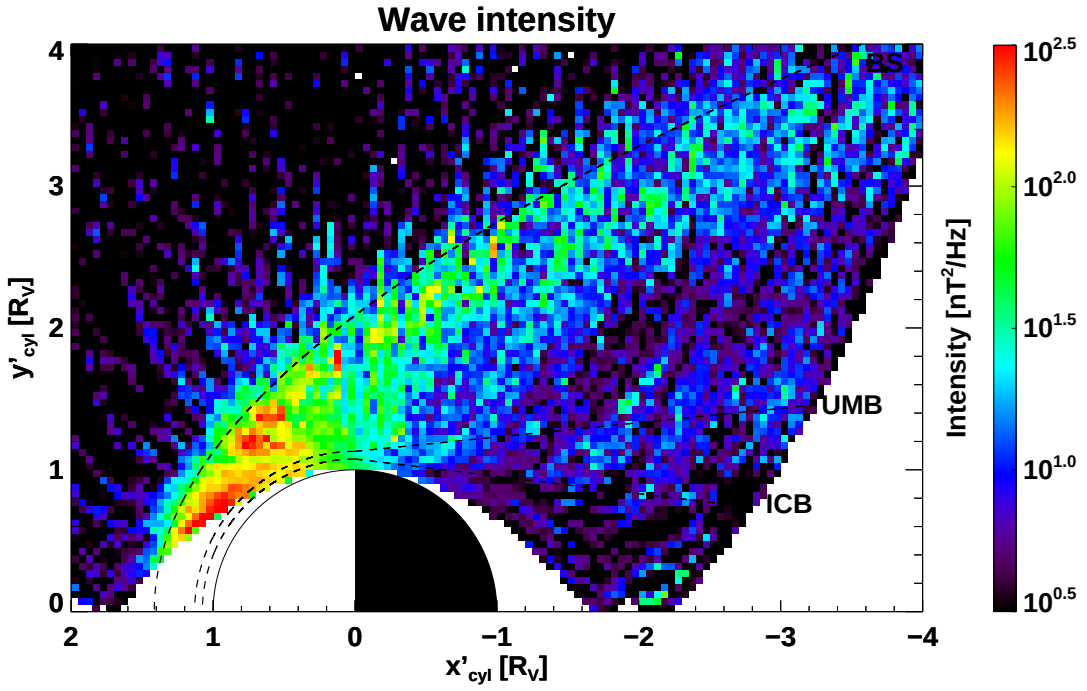

Fig. 8. Spatial distribution of the wave intensity. The intensity is enhanced in the entire dayside magnetosheath and drops rapidly towards the terminator. In the nightside magnetosheath the intensity has a reduced level. No significant intensity occurs in the upstream solar wind and the mantle and tail region.

Table 1. Observed spectral indices with its standard deviations of the mean in Venus' solar wind interaction region. The values in brackets represent the sample standard deviations.

region	component	spectral index
dayside magnetosheath	total	$-1.854 \pm 0.001\,(0.588)$
	transverse	$-1.783 \pm 0.001\,(0.622)$
	compressional	$-1.988 \pm 0.001\,(0.660)$
nightside magnetosheath	total	$-1.879 \pm 0.001\,(0.639)$
	transverse	$-1.851 \pm 0.001\,(0.696)$
	compressional	$-1.950 \pm 0.001\,(0.636)$
mantle	total	$-2.407 \pm 0.001\,(0.433)$
	transverse	$-2.417 \pm 0.001\,(0.491)$
	compressional	$-2.471 \pm 0.001\,(0.624)$
tail	total	$-2.407 \pm 0.001\,(0.390)$
	transverse	$-2.470 \pm 0.001\,(0.464)$
	compressional	$-2.406 \pm 0.001\,(0.625)$

intensity is enhanced in the entire dayside magnetosheath and drops rapidly at the terminator. Towards the nightside magnetosheath the transverse power increases and exceeds the compressional power in the majority of cases except for the regions close to the vicinity of the bow shock. The ellipticity is still moderate, but also in a few areas the ellipticity becomes lower and left-handed or right-handed senses of polarisation can locally be observed. A significant part of the angles between the propagation direction and the mean magnetic field has values below 45°, but they increase near the bow shock and the UMB. The wave intensity is significantly lower compared to the dayside magnetosheath, but in the vicinity of the bow shock areas of higher intensity are still present. The transverse and compressional power in the mantle and tail region are fairly mixed with a slight majority of areas in which the transverse power dominates. The ellipticity varies over a wider range compared to the magnetosheath and areas of locally dominated left-handed or right-handed polarisation also occur, but rather at larger distances from the planet. The wave vector directions have in most cases angles greater than 45° with respect to the mean magnetic field. The intensity is in the entire mantle and tail region at a very low level. In contrast, the upstream solar wind region is characterised by dominating transverse power with a broad spectrum of ellipticity values and various angles between the propagation direction of the waves and the mean field with no clear areas of enhanced wave intensity. The spectral indices (Table 1) indicate a turbulent behaviour of the magnetic field fluctuations at Venus. In particular, the magnetosheath reveals slightly smaller indices than expected

for hydrodynamic ($\alpha = -5/3$) and magnetohydrodynamic (MHD) turbulence ($\alpha = -3/2$) and the mantle and tail region even more smaller indices meaning that the spectral power decreases more rapidly there. The spectral slopes observed by Vörös et al. (2008a,b) for a case study along the Venus Express trajectory and a statistical analysis of 20 days in the magnetosheath (not close to boundaries) are $\alpha \approx -1$ (termed as noisy fluctuations), near the terminator and in the nightside near-planet wake $\alpha \approx -2.5$ (termed as wavy structures), and close to boundaries $\alpha \approx -1.6$ (termed as turbulent regions). Hence, our observations of a much longer time interval are rather similar in the tail and mantle region, but differ in the magnetosheath. Different behaviour of the transverse and compressional indices indicate that an anisotropy develops with increasing frequencies which tends to be most pronounced in the dayside magnetosheath.

Espley et al. (2004) presented a statistical study of low-frequency magnetic field oscillations in the Martian magnetosheath, the magnetic pileup region, and the tail using observations of the magnetometer/electron reflectometer (MAG/ER) experiment on board Mars Global Surveyor (MGS). Below the local proton gyrofrequency they found waves in the dayside magnetosheath which are predominantly compressional and elliptically polarised with wave vectors that have large angles relative to the mean magnetic field. These oscillations were identified as mirror mode fluctuations. In the nightside magnetosheath they observed waves which are predominantly transverse and elliptical, propagating at smaller angles relative to the mean field. The waves were associated with ion/ion-resonant instabilities arising from counter-streaming plasma populations like solar wind pickup ions of planetary origin. Waves in the Martian magnetic pileup region and tail have considerably smaller amplitudes with linear polarisation and oblique propagation directions. They may be a mixture of different wave modes. The intensity of the oscillations was not presented in their study.

Our dayside observations at Venus reveal similar results in comparison to the wave properties in the Martian magnetosheath, except for the fact that the compressional fluctuations are not dominating at Venus. Espley et al. (2004) interpret their observed fluctuations as mirror mode waves, but they also admit that this interpretation is in conflict with the observation of a moderate elliptical polarisation of the waves, as theoretical studies suggest that mirror modes are linearly polarised. But they argue that elliptically polarised mirror mode waves have also been observed in Earth's magnetosheath. Volwerk et al. (2008a,b) detected mirror mode-like structures in Venus' dayside magnetosheath so that the properties of mirror modes may give a contribution to our statistical results. On the other hand, Luhmann et al. (1983) suggested that magnetic field fluctuations may be generated in the vicinity of the quasi-parallel portion of the bow shock by plasma instabilities and are convected downstream through the magnetosheath. Indeed, this is an agreement with the results of numerical simulations by Winske (1986) who studied the origin of large magnetic fluctuations in the magnetosheath of Venus and concluded that the most likely source of these waves is the bow shock itself. But the numerical simulations have also shown that waves could be generated by direct interaction of the solar wind with oxygen ions of planetary origin which tends to generate right-handed polarised waves, whereas the bow shock related waves would generate left-handed polarised waves. However, the simulation by Winske (1986) is performed in an idealised situation and our results of the sense of polarisation can be subject to an uncertainty due to the Doppler shift. As already mentioned in Sect. 3.3 upward propagating waves could reverse their senses of polarisation. Assuming that the waves are mainly bow shock generated and propagate downstream one may conclude that right-handed and left-handed wave generation mechanisms are balanced as our observations show that the senses of polarisation are rather mixed. At Venus the average Parker spiral angle is about 35° (Luhmann et al., 1997). Thus, the most developed quasi-parallel bow shock geometry in the ecliptic plane (dusk sector) with angles between the bow shock normal $\boldsymbol{n}$ and the interplanetary magnetic field (IMF) $\boldsymbol{B}$ of less than 10°, we estimate to appear at moderate solar zenith angles (SZA's; the SZA is the angle between the x-axis and the line connecting the point of origin with a point on the bow shock in the VSO′ coordinate system) of about 30° to 70°. In our cylindrical coordinate system the wave intensity related to quasi-parallel bow shock processes would occur in the same angle range, but due to the averaging the wave intensity may be reduced. We notice a localisation of the majority of red-coloured bins in Fig. 8 between 30° and 70° SZA. Altogether, the enhanced wave intensity downstream of the bow shock is remarkable. Therefore, we refer a substantial part of the wave activity to bow shock related processes and interpret that, in particular, the wave generation could be associated with the quasi-parallel shock itself as also Luhmann et al. (1983) suggested. However, the bins showing the largest wave intensity at low SZA's are closer to the UMB than to the bow shock suggesting that wave sources may also exist in the magnetosheath and in the vicinity of the UMB, respectively. The generation of mirror mode waves in Earth's magnetosheath is believed to occur not only at the bow shock, but also within the magnetosheath (Tátrallyay and Erdős, 2002). The origin and evolution of mirror mode structures observed at Venus (Volwerk et al., 2008a,b) may be similar and mirror modes are thus a candidate for waves generated downstream of the bow shock. A differentiation between the quasi-parallel and quasi-perpendicular bow shock regions based on Venus Express measurements of the IMF direction is beyond the scope of this paper and will be subject of future work. A first case study has recently been presented by Du et al. (2009).

The wave properties of the nightside magnetosheaths at Venus and Mars also show similarities: at both planets the power or amplitude is more in the transverse direction than

in the compressional one, the oscillations tend to be elliptical, and the propagation directions are below 45° relative to the mean field. Espley et al. (2004) refer the observations at Mars to ion/ion-resonant instabilities.

Finally, the tail and mantle regions of Venus show a wider range of observations. This is also similar to the Martian case where a mixture of wave modes are believed to exist. Boundary related processes and current systems (e.g. the ionospheric current system) may become more important there and instabilities may cause a variety of wave modes.

The presented statistical analysis of the low-frequency magnetic field fluctuations reveals first-order results of the wave characteristics in specific regions. They show only the dominating waves properties in different interaction regions and provide a general picture of possible wave modes in Venus' solar wind interaction region. While much of our discussion assumes MHD wave modes, we note that more complex kinetic plasma models take account of temperature anisotropies and non-Maxwellian velocity distributions which lead to various micro-instabilities and additional waves modes. For anisotropic proton-electron plasmas Gary et al. (1993) argue several low-frequency plasma instabilities. For non-Maxwellian plasma distributions Gary (1991, 1993) also present possible wave generation mechanisms. Case studies give a detailed view of the wave modes and will be an interesting issue of future work using Venus Express data. In this paper we restrict our analysis to the statistical point of view, as it is motivated by a comparative study to Mars. The observations of the wave properties show generally results which emphasise the similarities of the interaction of the planets with the solar wind assuming that the observed wave properties are attributed to the same generation processes.

Concerning the post-terminator waves observed by Brace et al. (1983) at Venus, we do not see a relation to our observations at the moment since these waves are observed below 200 km altitude, while the lowest altitude of the Venus Express spacecraft was about 250 km in the data set we analysed. But Brace et al. (1983) discuss as one possible source of the waves turbulence at higher altitudes and thus it will be interesting to look whether this phenomenon and observations can be connected or not once data of lower altitudes are available.

4.2 Wave intensity and Alfvénic/magnetosonic boundary

One possibility to explain the localisation of enhanced wave activity in the dayside magnetosheath may be spatial variations of the Mach numbers in Venus' solar wind interaction region. The solar wind upstream of the bow shock is characterised by supersonic, super-Alfvénic, and supermagnetosonic velocities (e.g. Luhmann et al., 1997). The bow shock is a fast magnetosonic shock wave (e.g. Phillips and McComas, 1991) and thus the solar wind flow is slowed down to submagnetosonic velocities, when crossing the shock wave. Further downstream of the shock the flow should reach again supermagnetosonic velocities at a "magnetosonic" line similar to the so-called sonic line inferred from numerical simulations by Spreiter and Stahara (1980). A similar behaviour may occur for the Alfvén Mach number in MHD. Downstream of the bow shock also the Alfvén Mach number may become less than 1, because of the varying magnetic field strength, density, and temperature. In a sub-Alfvénic/submagnetosonic regime waves are not only convected by the flow, but can also propagate upstream and populate the entire region between the bow shock and an Alfvén or a magnetosonic line. In a super-Alfvénic/supermagnetosonic regime the wave energy transport is only in the direction of the background flow. Thus, the transition region from sub-Alfvénic/submagnetosonic to super-Alfvénic/supermagnetosonic flows could represent a reasonable boundary in the wave activity level. Without further knowledge of parameters like the plasma temperature and the density the location of such a boundary and the spatial distributions of the Mach numbers remain speculative for the moment. It can be investigated in more detail with a comprehensive plasma moment data set which is yet not provided by the Analyser of Space Plasmas and Energetic Atoms (ASPERA-4) on board the Venus Express spacecraft. However, an estimate of the Alfvén Mach number we determined on the basis of preliminary ASPERA-4 density and the magnetic field observations. It indicates an Alfvén Mach number greater than 1 in Venus' magnetosheath and thus waves with velocities up to the Alfvén velocity should be convected with the plasma flow.

4.3 Wave intensity along streamlines

As a further possibility to interpret the observed wave intensity distribution, we discuss the geometric effect on the decay of the waves with the hypothesis that a spatial variation of the wave intensity is due to varying distances between streamlines and the change of the flow velocity. Testing this hypothesis requires knowledge of the magnetosheath flow pattern. For this, we apply an analytical streamline model to describe the flow in the magnetosheath which allows us to trace the evolution of the intensity along different streamlines in the statistical sense. We use the model of a hydrodynamic, irrotational flow (e.g. Vallentine, 1967) past a cylinder for the dayside magnetosheath continued by a flow parallel to a straight line for the nightside. This model was already used successfully by Luhmann et al. (1983) tracing magnetic field fluctuations along streamlines back to the quasi-parallel portion of the bow shock. They also pointed out that the model streamlines are in good agreement with that of the gasdynamic model of Spreiter and Stahara (1980) for the solar wind interaction with Venus. We note here that the nightside mantle boundaries of Martinecz et al. (2009) are modelled in a different way than the dayside boundaries and a continuous

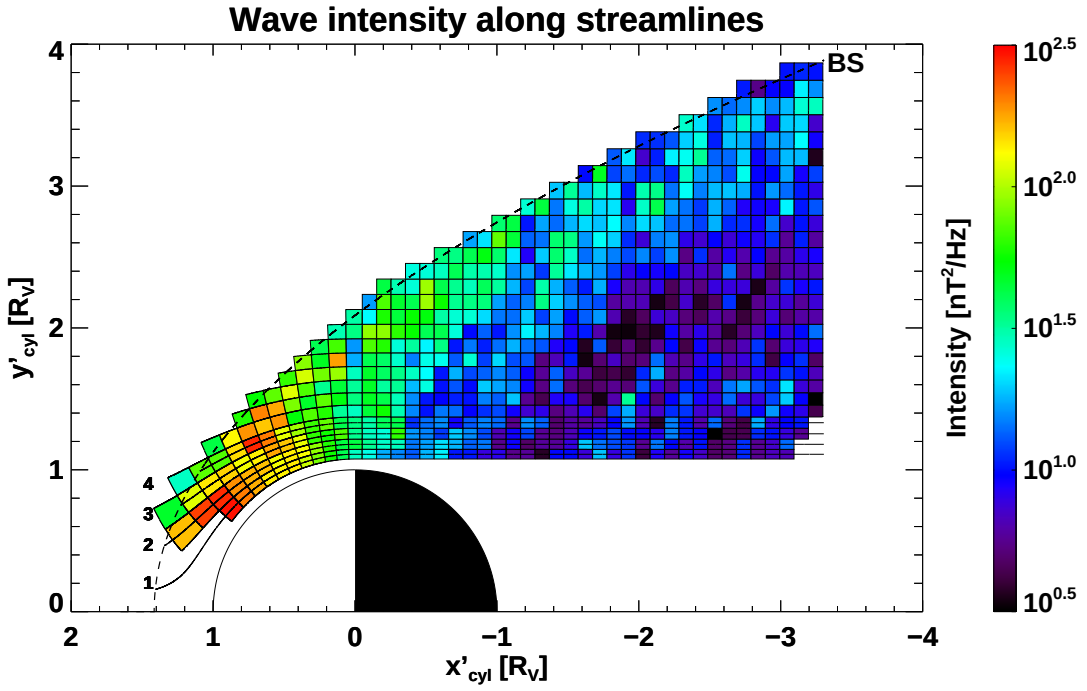

Fig. 9. Intensity along streamlines. The intensities connected to the different positions along any streamline are averaged over the neighbouring streamlines and velocity potential lines. Solid lines display magnetosheath streamlines which are also numbered.

transition is lacking at the terminator which cannot be reproduced by the analytical streamline model. As our focus lies on the dayside magnetosheath and the intensity on the nightside is generally much lower, no major deviations are expected by considering a straight streamline parallel to the x′-axis. The streamline functions Ψ are given as

$$\Psi_{\mathrm{d}} = vy'\left(1-\frac{r^2}{x'^2+y'^2}\right), \tag{5}$$

$$\Psi_{\mathrm{n}} = vy', \tag{6}$$

for the dayside (d) and the nightside (n), respectively. v is the nominal velocity (100 km/s), r is the radius of the obstacle, and x', y', z' are the Cartesian coordinates. The velocity vector is tangential to the streamline at all points (which is the definition of a streamline). Furthermore, we define the velocity potential functions Φ given as

$$\Phi_{\mathrm{d}} = vy'\left(1+\frac{r^2}{x'^2+y'^2}\right), \tag{7}$$

$$\Phi_{\mathrm{n}} = vx', \tag{8}$$

for the dayside and the nightside, respectively. The velocity potential lines are defined such that, when differentiated with respect to distance in any particular direction, it yields the velocity in that direction. The velocity potential lines are perpendicular to the streamlines.

Figure 9 shows the spatial distribution of the wave intensity connected to the streamlines. The intensity is averaged over two neighbouring streamlines and velocity potential lines.

Considering now a geometric effect on the wave intensity decay along a streamline $I(s)$ due to the varying velocity and cross sectional area, the continuity equation of a stationary flow as a function of the distance along the streamline s is given as

$$I(s)\,v(s)\,A(s) = \text{const.}, \tag{9}$$

where $v(s)$ is the velocity and $A(s)$ the cross sectional area of the flow line. Here, we assume that there is no wave source or sink in the magnetosheath. It is also assumed that the waves are generated in the bow shock region only and wave damping is restricted to frequencies close to the proton cyclotron frequency that is why the damping is not considered here. Equation (9) determines theoretically the evolution of the wave intensity and this can be compared to the observations. Here, the flow velocity $v(s)$ and the cross sectional area $A(s)$ can be estimated using the proposed flow model. Figure 10 shows examples of the evolution of the intensity along four different streamlines. The intensity evolution estimated from the continuity equation remains almost constant along the streamlines (solid lines), while the observed intensities (asterisk symbols) show a steeper decay. However, the observed wave intensity does not decrease monotonically

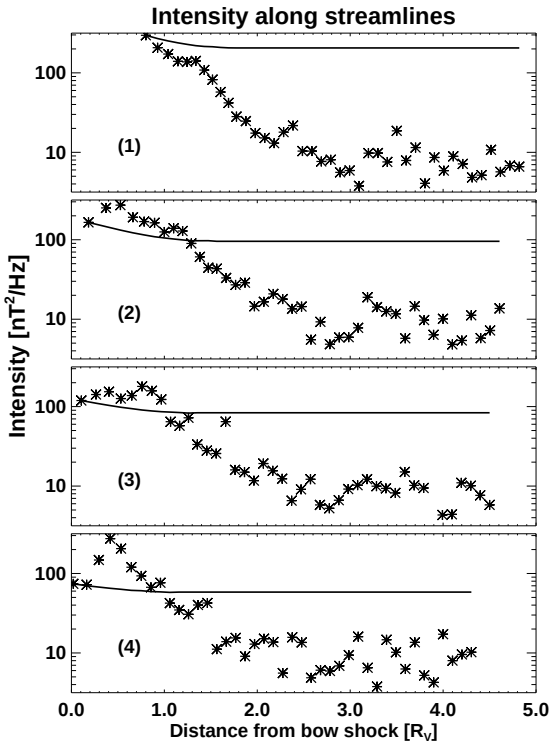

Fig. 10. Evolution of the intensity along different streamlines (the numbers (1) to (4) in the panels correspond to the streamlines in Fig. 9). The solid line denotes the calculated intensity function derived from the continuity equation (Eq. 9), while the asterisk symbols denote the observed intensities.

with increasing distance from the bow shock. At first, the intensity increases slightly and only then the decrease begins (streamlines 2 to 4; at streamline 1 no observations are available close to the bow shock) which may indicate also that a wave source further downstream of the bow shock exists. Generally, Fig. 10 suggests that the variations of the velocity and the cross sectional area along the streamlines are too small to account for the observed spatial decay of the wave intensity. Since the estimated intensities are almost constant, the changing velocity and cross sectional area play only a minor role in the evolution, even if one would assume that a wave source is located in the magnetosheath. Then, the initial value of the estimated intensity in Fig. 10 would change, but the almost constant curve shape would not be changed significantly. For this reason, we rule out the effect of velocity and cross section variations to explain the rapid spatial decay of the wave intensity in the magnetosheath.

4.4 Turbulence and wave energy transport

Magnetic field fluctuations in the magnetosheath are often interpreted to be in a turbulent state. We discuss finally wave energy transport due to turbulence in the magnetosheath as suggested by Luhmann et al. (1983) and Winske (1986). The hypothesis to be tested is if the energy loss of the fluctuations due to dissipation while convected with the flow through the magnetosheath is large enough in order to explain the spatial decay of the wave energy along magnetosheath streamlines.

The energy-decay laws for different types of turbulence are discussed comprehensively in the literature by Biskamp (2003) and Davidson (2004), known as freely evolving or decaying turbulence. A hydrodynamical example is wind-tunnel turbulence (Davidson, 2004) which is generated by an air stream passing through a grid. The interaction of the flow with the obstacle results in turbulence which is carried downstream by the mean flow. This situation is similar to that at Venus, as we relate the wave generation mainly to the bow shock. Hydrodynamic turbulence predicts that the time evolution of the fluctuation energy behaves like a power law

$$E \propto t^{-\lambda}, \tag{10}$$

where the exponent λ is characteristic for the turbulent system. According to Kolmogorov (1941) one can derive an exponent of $\lambda = 10/7$, while for MHD turbulence the exponent is $\lambda = 2/3$ (Biskamp, 2003). These exponents are derived under the assumption of self-similarity behaviour in turbulence. More complex models are also possible which consider various ratios of kinetic to magnetic energy and they provide further solutions of Eq. (10). Note that the exact solution of Eq. (10) is $E = E_0(t - t_0)^{-\lambda}$, where the constant t_0 is of the order of the initial eddy-turnover time and that is why the power law decay becomes visible only at sufficiently large times $t \gg t_0$ (Biskamp, 2003).

Since the flow velocity in the magnetosheath is supposed to be super-Alfvénic and the fluctuations are more Alfvénic (transverse), we relate the distance s along a streamline to the elapsed time since the bow shock crossing by using Taylor's hypothesis

$$t = \frac{s}{v(s)}. \tag{11}$$

We note that this a reasonably good approximation for not propagating waves like mirror modes or downstream propagating waves in the plasma frame of reference, but the time scale would increase in case of upward propagating waves and Taylor's hypothesis should be used with caution. The measured intensity I is proportional to the magnetic energy density E of the fluctuations in the frequency range 30 to 300 mHz if normalised by a constant C such that $E = CI$ with $C = N\Delta f(2\mu_0)^{-1}$ (N: Number of frequency samples over which has been averaged, Δf: frequency resolution in the spectra, μ_0: permeability of free space).

Figure 11 shows the evolution of the intensity with time after the bow shock crossing. A power law fitting to the decaying part of the observed intensity evolution gives a good agreement with the data. Some parts in the measurements show approximately a constant behaviour (data points closest to the bow shock, particularly in the third panel). They

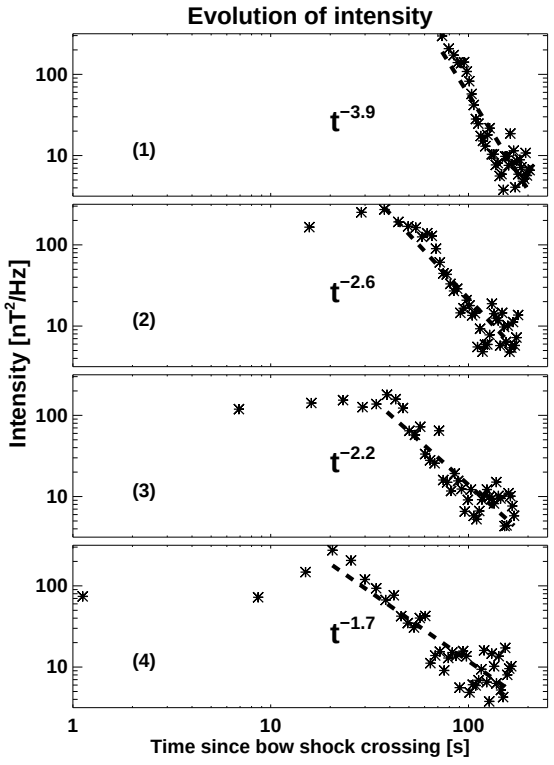

Fig. 11. Evolution of the intensity with time after the bow shock crossing (the numbers (1) to (4) in the panels correspond to the streamlines in Fig. 9). The x-axis is relabelled from Fig. 10 using Taylor's hypothesis. The asterisk symbols denote the observed intensities. The decaying part is fitted by a power law (dashed line).

may be related to the constant t_0 which is of the order of a few tens of seconds. The observed exponents λ vary from -1.7 to -3.9 and are steeper than the exponents predicted by theoretical models of turbulence, but nevertheless the observations exhibit the power law decay and it is suggestive of turbulent decay. Considering wave sources in the magnetosheath, the $t = 0$ point has not to be located necessarily at the bow shock, but can be located further downstream. This would shift the data in Fig. 11 to the left leading to a lower exponent of the power law. Then, the power law exponents would probably be more consistent with the theoretical exponents and therefore, one may consider further wave sources possible. Of course the theoretical models describe an idealised picture of turbulence (spatially unbounded, etc.) and a realistic model would be needed for a quantitative study (considering e.g. the magnetosheath geometry, the bow shock shape and the solar wind conditions). We note in this context that it is also worthwhile to consider in future studies, performing a more detailed discussion on turbulent processes, the spatial distribution and the evolution of the relative amplitude $\Delta B/B$.

5 Conclusions

We performed a statistical analysis of low-frequency magnetic field fluctuations in the frequency range 30 to 300 mHz in the Venusian solar wind interaction region. The magnetic field data set was obtained by the fluxgate magnetometer on board the Venus Express spacecraft. The observations cover the low-altitude magnetosheath as well as the mid-magnetotail. The observations reveal similar wave properties in the magnetosheaths of Venus and Mars as well as their tail regions, suggesting a similar solar wind interaction between the two planets. However, only a global picture of the dominating wave properties is provided which is suitable to compare the observations at both planets, but we are not resolving individual wave modes. This is left to future studies. We also note that the wave propagation directions and the wave properties in the plasma frame of reference are not determined in our measurements and this makes it difficult to get clearer results. This is due to measurements from a single spacecraft only.

The wave intensity reaches a maximum in the dayside magnetosheath and drops rapidly towards the terminator region. The further regions do not show significant wave intensities. Different hypotheses have been considered in order to explain our observation. The influence of varying Mach numbers can not be evaluated accurately at the moment. It has to be studied in more detail in the future with a comprehensive plasma moment data set. A geometric effect plays only a minor role. A reasonable explanation is freely evolving or decaying turbulence, because of the power law behaviour. But the quantitative agreement is poor with the freely decaying turbulence model which may probably be improved by taking wave generation in the magnetosheath into account. On the other hand, further mechanisms like damping could be responsible for the loss of energy. Perhaps the decrease in the magnetic field fluctuations may be compensated by a relative increase in the electric field fluctuation as in high-frequency phenomena in the solar wind (Bale et al., 2005). Unfortunately, this can not be verified by Venus Express, since the spacecraft is not equipped with an electric field detector. Also, a dissipation process could take place like Landau or cyclotron damping. This will be studied using plasma moment data once they are available soon.

In summary, we conclude that the observations suggest the convection of waves by the plasma flow. Doubtless, waves are generated at the bow shock or in its vicinity. But the observations indicate also wave sources within the magnetosheath and thus it may occur that beside the bow shock region waves are also generated within the magnetosheath and the vicinity of the UMB, respectively.

Acknowledgements. This work was financially supported by the Deutsche Forschungsgemeinschaft under contract MO 539/17-1. Part of the work was financially supported by the German Ministerium für Wirtschaft und Technologie and the Deutsches Zentrum für Luft- und Raumfahrt under grant 50QP0402.

Topical Editor R. Nakamura thanks J. Espley and another anonymous referee for their help in evaluating this paper.

References

Acuña, M. H., Connerney, J. E. P., Wasilewski, P., Lin, R. P., Anderson, K. A., Carlson, C. W., McFadden, J., Curtis, D. W., Mitchell, D., Rème, H., Mazelle, C., Sauvaud, J. A., d'Uston, C., Cros, A., Medale, J. L., Bauer, S. J., Cloutier, P., Mayhew, M., Winterhalter, D., and Ness, N. F.: Magnetic Field and Plasma Observations at Mars: Initial Results of the Mars Global Surveyor Mission, Science, 279, 1676–1680, doi:10.1126/science.279.5357.1676, 1998.

Arthur, C. W., McPherron, R. L., and Means, J. D.: A comparative study of three techniques for using the spectral matrix in wave analysis, Radio Sci., 11, 833–845, doi:10.1029/RS011i010p00833, 1976.

Bale, S. D., Kellogg, P. J., Mozer, F. S., Horbury, T. S., and Rème, H.: Measurement of the Electric Fluctuation Spectrum of Magnetohydrodynamic Turbulence, Phys. Rev. Lett., 94, 215002, doi:10.1103/PhysRevLett.94.215002, 2005.

Biskamp, D.: Magnetohydrodynamic Turbulence, Cambridge Univ. Press, Cambridge, 2003.

Brace, L. H., Elphic, R. C., Curtis, S. A., and Russell, C. T.: Wave structure in the Venus ionosphere downstream of the terminator, Geophys. Res. Lett., 10, 1116–1119, doi:10.1029/GL010i011p01116, 1983.

Cloutier, P. A., Law, C. C., Crider, D. H., Walker, P. W., Chen, Y., Acuña, M. H., Connerney, J. E. P., Lin, R. P., Anderson, K. A., Mitchell, D. L., Carlson, C. W., McFadden, J., Brain, D. A., Rème, H., Mazelle, C., Sauvaud, J. A., d'Uston, C., Vignes, D., Bauer, S. J., and Ness, N. F.: Venus-like interaction of the solar wind with Mars, Geophys. Res. Lett., 26, 2685–2688, doi:10.1029/1999GL900591, 1999.

Davidson, P. A.: Turbulence: An introduction for scientists and engineers, Oxford Univ. Press, New York, 2004.

Delva, M., Zhang, T. L., Volwerk, M., Magnes, W., Russell, C. T., and Wei, H. Y.: First upstream proton cyclotron wave observations at Venus, Geophys. Res. Lett., 35, L3105, doi:10.1029/2007GL032594, 2008a.

Delva, M., Zhang, T. L., Volwerk, M., Russell, C. T., and Wei, H. Y.: Upstream proton cyclotron waves at Venus, Planet. Space Sci., 56, 1293–1299, doi:10.1016/j.pss.2008.04.014, 2008b.

Delva, M., Zhang, T. L., Volwerk, M., Vörös, Z., and Pope, S. A.: Proton cyclotron waves in the solar wind at Venus, J. Geophys. Res., 113, E00B06, doi:10.1029/2008JE003148, 2008c.

Du, J., Zhang, T. L., Wang, C., Volwerk, M., Delva, M., and Baumjohann, W.: Magnetosheath fluctuations at Venus for two extreme orientations of the interplanetary magnetic field, Geophys. Res. Lett., 36, L09102, doi:10.1029/2009GL037725, 2009.

Espley, J. R., Cloutier, P. A., Brain, D. A., Crider, D. H., and Acuña, M. H.: Observations of low-frequency magnetic oscillations in the Martian magnetosheath, magnetic pileup region, and tail, J. Geophys. Res., 109, A07213, doi:10.1029/2003JA010193, 2004.

Gary, S. P.: Electromagnetic ion/ion instabilities and their consequences in space plasmas: A review, Space Sci. Rev., 56, 373–415, doi:10.1007/BF00196632, 1991.

Gary, S. P.: Theory of Space Plasma Microinstabilities, Cambridge atmospheric and space science series, Cambridge Univ. Press, New York, 1993.

Gary, S. P., Fuselier, S. A., and Anderson, B. J.: Ion anisotropy instabilities in the magnetosheath, J. Geophys. Res., 98, 1481–1488, doi:10.1029/92JA01844, 1993.

Glassmeier, K.-H. and Espley, J.: ULF Waves in Planetary Magnetospheres, in: Magnetospheric ULF Waves: Synthesis and New Directions, edited by: Takahashi, K., Chi, P. J., Denton, R. E., and Lysak, R. L., Geophysical Monograph Series 169, pp. 341–359, American Geophysical Union, Washington, D.C., 2006.

Grebowsky, J. M., Crider, D. H., Intriligator, D. S., Hartle, R. E., and Acuña, M. H.: Venus/Mars pickup ions and ionosheath wave structures, Adv. Space Res., 33, 176–181, doi:10.1016/j.asr.2003.04.014, 2004.

Hoppe, M. M. and Russell, C. T.: Plasma rest frame frequencies and polarizations of the low-frequency upstream waves: ISEE 1 and 2 observations, J. Geophys. Res., 88, 2021–2027, doi:10.1029/JA088iA03p02021, 1983.

Huba, J. D. and Strangeway, R. J.: Plasma wave phenomena at Venus, in: Venus II: Geology, Geophysics, Atmosphere, and Solar Wind Environment, edited by Bougher, S. W., Hunten, D. M., and Philips, R. J., pp. 95–124, The Univ. of Arizona Press, Tucson, 1997.

Kolmogorov, A. N.: Dissipation of energy in the locally isotropic turbulence, Dokl. Akad. Nauk SSSR, 32, 19–21, (reprinted in P. Roy. Soc. A, 434, 15-17, 1991), 1941.

Luhmann, J. G.: The solar wind interaction with Venus, Space Sci. Rev., 44, 241–306, doi:10.1007/BF00200818, 1986.

Luhmann, J. G.: The inner magnetosheath of Venus: An analogue for Earth?, J. Geophys. Res., 100, 12035–12045, doi:10.1029/94JA02862, 1995.

Luhmann, J. G., Tatrallyay, M., Russell, C. T., and Winterhalter, D.: Magnetic field fluctuations in the Venus magnetosheath, Geophys. Res. Lett., 10, 655–658, doi:10.1029/GL010i008p00655, 1983.

Luhmann, J. G., Brecht, S. H., Spreiter, J. R., Stahara, S. S., Steinolfson, R. S., and Nagy, A. F.: Global models of the solar wind interaction with Venus, in: Venus II: Geology, Geophysics, Atmosphere, and Solar Wind Environment, edited by: Bougher, S. W., Hunten, D. M., and Philips, R. J., pp. 33–59, The Univ. of Arizona Press, Tucson, 1997.

Martinecz, C., Fränz, M., Woch, J., Krupp, N., Roussos, E., Dubinin, E., Motschmann, U., Barabash, S., Lundin, R., Holmström, M., Andersson, H., Yamauchi, M., Grigoriev, A., Futaana, Y., Brinkfeldt, K., Gunell, H., Frahm, R. A., Winningham, J. D., Sharber, J. R., Scherrer, J., Coates, A. J., Linder, D. R., Kataria, D. O., Kallio, E., Sales, T., Schmidt, W., Riihela, P., Koskinen, H. E. J., Kozyra, J. U., Luhmann, J., Russell, C. T., Roelof, E. C., Brandt, P., Curtis, C. C., Hsieh, K. C., Sandel, B. R., Grande, M., Sauvaud, J.-A., Fedorov, A., Thocaven, J.-J., Mazelle, C., McKenna-Lawler, S., Orsini, S., Cerulli-Irelli, R., Maggi, M., Mura, A., Milillo, A., Wurz, P., Galli, A., Bochsler, P., Asamura, K., Szego, K., Baumjohann, W., Zhang, T. L., and Lammer, H.: Location of the bow shock and ion composition boundaries at Venus – initial determinations from Venus Express ASPERA-4, Planet. Space Sci., 56, 780–784, doi:10.1016/j.pss.2007.07.007, 2008.

Martinecz, C., Boesswetter, A., Fränz, M., Roussos, E., Woch, J., Krupp, N., Dubinin, E., Motschmann, U., Wiehle, S., Simon, S., Barabash, S., Lundin, R., Zhang, T. L., Lammer, H., Licht-

enegger, H., and Kulikov, Y.: Plasma environment of Venus: Comparison of Venus Express ASPERA-4 measurements with 3-D hybrid simulations, J. Geophys. Res., 114, E00B30, doi:10.1029/2008JE003174, (correction in J. Geophys. Res., 114, E00B98, doi:10.1029/2009JE003377, 2009), 2009.

McPherron, R. L., Russell, C. T., and Coleman Jr., P. J.: Fluctuating Magnetic Fields in the Magnetosphere – II. ULF Waves, Space Sci. Rev., 13, 411–454, doi:10.1007/BF00219165, 1972.

Means, J. D.: Use of the Three-Dimensional Covariance Matrix in Analyzing the Polarization Properties of Plane Waves, J. Geophys. Res., 77, 5551–5559, doi:10.1029/JA077i028p05551, 1972.

Orlowski, D. S., Russell, C. T., Krauss-Varban, D., and Omidi, N.: A test of the Hall-MHD model: Application to low-frequency upstream waves at Venus, J. Geophys. Res., 99, 169–178, doi:10.1029/93JA01808, 1994.

Phillips, J. L. and McComas, D. J.: The magnetosheath and magnetotail of Venus, Space Sci. Rev., 55, 1–80, doi:10.1007/BF00177135, 1991.

Russell, C. T. (Ed.): Venus Aeronomy, Kluwer Academic Publishers, Dordrecht, Boston, London, (reprinted from Space Sci. Rev., 55(1–4), 1991), 1991.

Russell, C. T., Snare, R. C., Means, J. D., and Elphic, R. C.: Pioneer Venus Orbiter fluxgate magnetometer, IEEE T. Geosci. Remote, 18, 32–35, doi:10.1109/TGRS.1980.350256, 1980.

Samson, J. C.: Descriptions of the Polarization States of Vector Processes: Applications to ULF Magnetic Fields, Geophys. J. Roy. Astr. S., 34, 403–419, doi:10.1111/j.1365-246X.1973.tb02404.x, 1973.

Song, P. and Russell, C. T.: Time Series Data Analyses in Space Physics, Space Sci. Rev., 87, 387–463, doi:10.1023/A:1005035800454, 1999.

Sonnerup, B. U. Ö. and Cahill, Jr., L. J.: Magnetopause Structure and Attitude from Explorer 12 Observations, J. Geophys. Res., 72, 171–183, doi:10.1029/JZ072i001p00171, 1967.

Spreiter, J. R. and Stahara, S. S.: Solar wind flow past Venus - Theory and comparisons, J. Geophys. Res., 85, 7715–7738, doi:10.1029/JA085iA13p07715, 1980.

Strangeway, R. J.: Plasma waves at Venus, Space Sci. Rev., 55, 275–316, doi:10.1007/BF00177139, 1991.

Strangeway, R. J.: Plasma waves and electromagnetic radiation at Venus and Mars, Adv. Space Res., 33, 1956–1967, doi:10.1016/S0273-1177(04)00019-5, 2004.

Strangeway, R. J. and Crawford, G. K.: VLF waves in the foreshock, Adv. Space Res., 15, 29–42, doi:10.1016/0273-1177(94)00147-S, 1995.

Tátrallyay, M. and Erdős, G.: The evolution of mirror mode fluctuations in the terrestrial magnetosheath, Planet. Space Sci., 50, 593–599, 2002.

Titov, D. V., Svedhem, H., McCoy, D., Lebreton, J.-P., Barabash, S., Bertaux, J.-L., Drossart, P., Formisano, V., Haeusler, B., Korablev, O. I., Markiewicz, W., Neveance, D., Petzold, M., Piccioni, G., Zhang, T. L., Taylor, F. W., Lellouch, E., Koschny, D., Witasse, O., Warhaut, M., Acomazzo, A., Rodrigues-Cannabal, J., Fabrega, J., Schirmann, T., Clochet, A., and Coradini, M.: Venus Express: Scientific goals, instrumentation, and scenario of the mission, Cosmic Res., 44, 334–348, doi:10.1134/S0010952506040071, 2006.

Vallentine, H. R.: Applied hydrodynamics, Butterworths, London, 2nd edn., 1967.

Vörös, Z., Zhang, T. L., Leubner, M. P., Volwerk, M., Delva, M., Baumjohann, W., and Kudela, K.: Magnetic fluctuations and turbulence in the Venus magnetosheath and wake, Geophys. Res. Lett., 35, L11102, doi:10.1029/2008GL033879, 2008a.

Vörös, Z., Zhang, T. L., Leubner, M. P., Volwerk, M., Delva, M., and Baumjohann, W.: Intermittent turbulence, noisy fluctuations, and wavy structures in the Venusian magnetosheath and wake, J. Geophys. Res., 113, E00B21, doi:10.1029/2008JE003159, (correction in J. Geophys. Res., 114, E00B35, doi:10.1029/2009JE003331, 2009), 2008b.

Volwerk, M., Zhang, T. L., Delva, M., Vörös, Z., Baumjohann, W., and Glassmeier, K.-H.: Mirror-mode-like structures in Venus' induced magnetosphere, J. Geophys. Res., 113, E00B16, doi:10.1029/2008JE003154, 2008a.

Volwerk, M., Zhang, T. L., Delva, M., Vörös, Z., Baumjohann, W., and Glassmeier, K.-H.: First identification of mirror mode waves in Venus' magnetosheath?, Geophys. Res. Lett., 35, L12 204, doi:10.1029/2008GL033621, 2008b.

Winske, D.: Origin of large magnetic fluctuations in the magnetosheath of Venus, J. Geophys. Res., 91, 11951–11957, doi:10.1029/JA091iA11p11951, 1986.

Zhang, T. L., Baumjohann, W., Delva, M., Auster, H.-U., Balogh, A., Russell, C. T., Barabash, S., Balikhin, M., Berghofer, G., Biernat, H. K., Lammer, H., Lichtenegger, H., Magnes, W., Nakamura, R., Penz, T., Schwingenschuh, K., Vörös, Z., Zambelli, W., Fornaçon, K.-H., Glassmeier, K.-H., Richter, I., Carr, C., Kudela, K., Shi, J. K., Zhao, H., Motschmann, U., and Lebreton, J.-P.: Magnetic field investigation of the Venus plasma environment: Expected new results from Venus Express, Planet. Space Sci., 54, 1336–1343, doi:10.1016/j.pss.2006.04.018, 2006.

Zhang, T. L., Delva, M., Baumjohann, W., Volwerk, M., Russell, C. T., Barabash, S., Balikhin, M., Pope, S., Glassmeier, K.-H., Kudela, K., Wang, C., Vörös, Z., and Zambelli, W.: Initial Venus Express magnetic field observations of the Venus bow shock location at solar minimum, Planet. Space Sci., 56, 785–789, doi:10.1016/j.pss.2007.09.012, 2008a.

Zhang, T. L., Delva, M., Baumjohann, W., Volwerk, M., Russell, C. T., Barabash, S., Balikhin, M., Pope, S., Glassmeier, K.-H., Wang, C., and Kudela, K.: Initial Venus Express magnetic field observations of the magnetic barrier at solar minimum, Planet. Space Sci., 56, 790–795, doi:10.1016/j.pss.2007.10.013, 2008b.

Zhang, T. L., Delva, M., Baumjohann, W., Volwerk, M., Russell, C. T., Wei, H. Y., Wang, C., Balikhin, M., Barabash, S., Auster, H.-U., and Kudela, K.: Induced magnetosphere and its outer boundary at Venus, J. Geophys. Res., 113, E00B20, doi:10.1029/2008JE003215, 2008c.